Cite as: T. M. Karg *et al.*, *Science*
10.1126/science.abb0328 (2020).

# Light-mediated strong coupling between a mechanical oscillator and atomic spins 1 meter apart

**Thomas M. Karg[1], Baptiste Gouraud[1]*, Chun Tat Ngai[1], Gian-Luca Schmid[1], Klemens Hammerer[2], Philipp Treutlein[1]†**

[1]Department of Physics and Swiss Nanoscience Institute, University of Basel, 4056 Basel, Switzerland. [2]Institute for Theoretical Physics and Institute for Gravitational Physics (Albert Einstein Institute), Leibniz Universität Hannover, 30167 Hannover, Germany.

*Present address: iXblue, 34 rue de la Croix de Fer, 78105 Saint-Germain-en-Laye, France.

†Corresponding author. Email: philipp.treutlein@unibas.ch

**Engineering strong interactions between quantum systems is essential for many phenomena of quantum physics and technology. Typically, strong coupling relies on short-range forces or on placing the systems in high-quality electromagnetic resonators, restricting the range of the coupling to small distances. We use a free-space laser beam to strongly couple a collective atomic spin and a micromechanical membrane over a distance of 1 meter in a room-temperature environment. The coupling is highly tunable and allows the observation of normal-mode splitting, coherent energy exchange oscillations, two-mode thermal noise squeezing and dissipative coupling. Our approach to engineer coherent long-distance interactions with light makes it possible to couple very different systems in a modular way, opening up a range of opportunities for quantum control and coherent feedback networks.**



Many of the recent breakthroughs in quantum science and technology rely on engineering strong, controllable interactions between quantum systems. In particular, Hamiltonian interactions that generate reversible, bidirectional coupling play an important role for creating and manipulating nonclassical states in quantum metrology (*1*), simulation (*2*), and information processing (*3*). For systems in close proximity, strong Hamiltonian coupling is routinely achieved, prominent examples being atom-photon coupling in cavity quantum electrodynamics (*4*) and coupling of trapped ions (*5*) or solid-state spins (*6*) via short-range electrostatic or magnetic forces. At macroscopic distances, however, the observation of strong Hamiltonian coupling is not only hampered by a severe drop in the interaction strength, but also by the fact that it becomes increasingly difficult to prevent information leakage from the systems to the environment, which renders the interaction dissipative (*7*). Overcoming these challenges would make Hamiltonian interactions available for reconfigurable long-distance coupling in quantum networks (*4*) and hybrid quantum systems (*8*, *9*), which so far employ mostly measurement-based or dissipative interactions.

A promising strategy to reach this goal uses one-dimensional waveguides or free-space laser beams over which quantum systems can couple via the exchange of photons. Such cascaded quantum systems (*10*) have attracted interest in the context of chiral quantum optics (*11*, *12*) and waveguide quantum-electrodynamics (*13*). A fundamental challenge in this approach is that the same photons that generate the coupling eventually leak out, thus allowing the systems to decohere at an equal rate. For this reason, light-mediated coupling is mainly seen today as a means for unidirectional state-transfer (*14*–*16*), or entanglement generation by collective measurement (*17*–*19*) or dissipation (*20*). Decoherence by photon loss can be suppressed if the waveguide is terminated by mirrors to form a high quality resonator, which has enabled coherent coupling of superconducting qubits (*21*, *22*), atoms (*23*), or atomic mechanical oscillators (*24*) in mesoscopic setups. However, stability constraints and bandwidth limitations make it difficult to extend resonator-based approaches to larger distances. Strong bidirectional Hamiltonian coupling mediated by light over a truly macroscopic distance has so far remained elusive.

We pursue an alternative approach to realize long-distance Hamiltonian interactions which relies on connecting two systems by a laser beam in a loop geometry (*25*, *26*). Through the loop the systems can exchange photons, realizing a bidirectional interaction. Moreover, the loop leads to an interference of quantum noise introduced by the light field. For any system that couples to the light twice and with opposite phase, quantum noise interferes destructively and associated decoherence is suppressed. At the same time information about that system is erased from the output field. In this way the coupled systems can effectively be closed to the environment, even though the light field mediates strong interactions between them. Since the coupling is mediated by light, it allows systems of different physical nature to be connected over macroscopic distances. Furthermore, by manipulating the light field in between the systems, one can reconfigure the interaction without having to modify the quantum systems themselves. These features will be useful for quantum networking (*4*).

We use this scheme to couple a collective atomic spin and a micromechanical membrane held in separate vacuum chambers, realizing a hybrid atom-optomechanical system (*8*). First experiments with such setups recently demonstrated sympathetic cooling (*27*, *28*), quantum back-action evading measurement (*29*) and entanglement (*30*). Here, we realize strong Hamiltonian coupling and demonstrate the versatility of light-mediated interactions: we engineer beam-splitter and parametric-gain Hamiltonians and switch from Hamiltonian to dissipative coupling by applying a phase shift to the light field between the systems. This high level of control in a modular setup gives access to a unique toolbox for designing hybrid quantum systems (*9*) and coherent feedback loops for advanced quantum control strategies (*31*).

## Description of the coupling scheme

In the experimental setup (Fig. 1A) (*32*), the atomic ensemble consists of $N = 10^7$ laser-cooled Rubidium-87 atoms in an optical dipole trap. The atoms form a collective spin $\mathbf{F} = \sum_{i=1}^{N} \mathbf{f}^{(i)}$ with $\mathbf{f}^{(i)}$ being the $f = 2$ ground state spin vector of atom $i$. Optical pumping polarises $\mathbf{F}$ along an external magnetic field $\mathbf{B}_0$ in the $x$-direction such that the spin acquires a macroscopic orientation $\bar{F}_x = -fN$. The small-amplitude dynamics of the transverse spin components $F_y$, $F_z$ are well approximated by a harmonic oscillator (*33*) with position $X_s = F_z / \sqrt{|\bar{F}_x|}$ and momentum $P_s = F_y / \sqrt{|\bar{F}_x|}$. It oscillates at the Larmor frequency $\Omega_s \propto B_0$, which is tuned by the magnetic field strength. A feature of the spin system is that it can realize such an oscillator with either positive or negative effective mass (*29*, *34*). This is achieved by reversing the orientation of $\mathbf{F}$ with respect to $\mathbf{B}_0$, which reverses the sense of rotation of the oscillator in the $X_s$, $P_s$-plane (Fig. 1B). This feature allows us to realize different Hamiltonian dynamics with the spin coupled to the membrane.

The spin interacts with the coupling laser beam through an off-resonant Faraday interaction (*33*) $H_s = 2\hbar\sqrt{\Gamma_s/\bar{S}_x}\,X_s S_z$, which couples $X_s$ to the polarization state of the light, described by the Stokes vector $\mathbf{S}$. Initially, the laser is linearly polarized along $x$ with $\bar{S}_x = \Phi_L/2$, where $\Phi_L$ is the photon flux. The strength of the atom-light coupling depends on the spin measurement rate $\Gamma_s \propto d_0\Phi_L/\Delta_a^2$, which is proportional to the optical depth $d_0 \approx 300$ of the atomic ensemble (*32*). Choosing a large laser-atom detuning $\Delta_a = -2\pi \times 80$ GHz suppresses spontaneous photon scattering while maintaining a sizable coupling.

The mechanical oscillator is the (2, 2) square drum mode of a silicon-nitride membrane at a vibrational frequency of $\Omega_m = 2\pi \times 1.957$ MHz with a quality factor of $1.3 \times 10^6$ (*35*). It is placed in a short single-sided optical cavity to enhance the optomechanical interaction while maintaining a large cavity bandwidth for fast and efficient coupling to the external light field. Radiation pressure couples the membrane displacement $X_m$ to the amplitude fluctuations $X_L$ of the light entering the cavity on resonance, with Hamiltonian $H_m = 2\hbar\sqrt{\Gamma_m}\,X_m X_L$ (*36*). Here, we defined the optomechanical measurement rate $\Gamma_m = (4g_0/\kappa)^2\Phi_m$ that depends on the vacuum optomechanical coupling constant $g_0$, cavity linewidth $\kappa$, and photon flux $\Phi_m$ entering the cavity (*32*). In the present setup, the optomechanical cavity is mounted in a room temperature vacuum chamber, making thermal noise the dominant noise source of the experiment.

The light-field mediates a bidirectional coupling between spin and membrane. A spin displacement $X_s$ is mapped by $H_s$ to a polarization rotation $S_y = 2\sqrt{\Gamma_s\bar{S}_x}\,X_s$ of the light. A polarization interferometer (Fig. 1A) converts this to an amplitude modulation $X_L \approx S_y/\sqrt{\bar{S}_x}$ at the optomechanical cavity, resulting in a force $\dot{P}_m = -4\sqrt{\Gamma_m\Gamma_s}\,X_s$ on the membrane. Conversely, a membrane displacement $X_m$ is turned by $H_m$ into a phase-modulation $P_L = -2\sqrt{\Gamma_m}\,X_m$ of the cavity output field. The interferometer converts this to a polarization rotation $S_z \approx \sqrt{\bar{S}_x}\,P_L$, resulting in a force $\dot{P}_s = 4\sqrt{\Gamma_s\Gamma_m}\,X_m$ on the spin. A small angle between the laser beams in the two atom-light interactions prevents light from going once more to the membrane. Consequently, the cascaded setup promotes a bidirectional spin-membrane coupling. A fully quantum mechanical treatment (*32*) confirms this picture and predicts a spin-membrane coupling strength $g = (\eta^2 + \eta^4)\sqrt{\Gamma_s\Gamma_m}$, accounting for an effective optical power transmission $\eta^2 \approx 0.8$ between the systems.

The light-mediated interaction can be thought of as a feedback loop that transmits a spin excitation to the membrane, whose response then acts back on the spin, and vice versa (Fig. 1B). After one round-trip, the initial signal has acquired a phase $\phi$, the loop phase. The discussion above refers to a vanishing loop phase $\phi = 0$ and shows that the forces $\dot{P}_m = -2gX_s$ and $\dot{P}_s = +2gX_m$ differ in their relative sign. Such a coupling is non-conservative and cannot arise from a Hamiltonian interaction. With full access to the laser beams, we can tune the loop phase by inserting a half-wave plate (HWP) in the path from the membrane back to the atoms, which rotates the Stokes vector by an angle $\phi = \pi$ about $S_x$. This inverts both $S_y$ and $S_z$, which carry the spin and membrane signals respectively, thus switching the dynamics to a fully Hamiltonian force, $\dot{P}_m = -2gX_s$ and $\dot{P}_s = -2gX_m$.

All these phenomena are unified in a rigorous quantum-mechanical theory (*26*) of the cascaded light-mediated coupling, which also correctly describes the dynamics for an arbitrary loop phase. It allows us to describe the effective dynamics of the coupled spin-membrane system with density operator $\rho$ by a Markovian master equation

$$\dot{\rho} = \frac{1}{i\hbar}\left[H_0 + H_{\text{eff}}, \rho\right] - \frac{1}{2}\left(J^\dagger J\rho + \rho J^\dagger J\right) + J\rho J^\dagger \qquad (1)$$

Here, we neglect optical loss and light propagation delay between the systems for brevity. The dynamics consist of a unitary part with free harmonic oscillator Hamiltonian $H_0 = \sum_{i=s,m} \hbar\Omega_i \left(X_i^2 + P_i^2\right)/2$ and effective interaction Hamiltonian $H_{\text{eff}} = (1-\cos\phi)\hbar g X_s X_m + 2\sin(\phi)\hbar\Gamma_s X_s^2$, and a dissipative part with collective jump operator $J = \sqrt{2\Gamma_m} X_m + i\left[1+\exp(i\phi)\right]\sqrt{2\Gamma_s} X_s$. Next to the coherent spin-membrane coupling, $H_{\text{eff}}$ also includes a spin self-interaction which vanishes for the specific cases $\phi = 0, \pi$ considered here. The jump operator contains a constant membrane term and a spin term that is modulated by $\phi$ due to interference of the two spin-light interactions. From the dependence of $H_{\text{eff}}$ and $J$ on $\phi$, it is clear that $\phi = 0$ corresponds to vanishing Hamiltonian coupling and maximum dissipative coupling. Accordingly, we refer to $\phi = 0$ as the dissipative regime. On the other hand, $\phi = \pi$ maximizes the coherent spin-membrane coupling in $H_{\text{eff}}$ and at the same time leads to destructive interference of the spin term in $J$, we thus call $\phi = \pi$ the Hamiltonian regime. Both regimes will be experimentally explored in the following, each with the atomic spin realizing either a positive- or negative-mass oscillator. This gives rise to a whole range of different dynamics in a single system, which can be harnessed for different purposes in quantum technology.

## Results

### *Normal-mode splitting*

We first investigate the light-mediated coupling in the Hamiltonian regime ($\phi = \pi$) and with the spin realizing a positive-mass oscillator. At a magnetic field of $B_0 = 2.81$ G the spin is tuned into resonance with the membrane ($\Omega_s = \Omega_m$). In this configuration, the resonant terms in $H_{\text{eff}}$ realize a beam-splitter interaction $H_{\text{BS}} = \hbar g\left(b_s^\dagger b_m + b_m^\dagger b_s\right)$, which generates state swaps between the two systems. Here $b_s = \left(X_s + iP_s\right)/\sqrt{2}$ and $b_m = \left(X_m + iP_m\right)/\sqrt{2}$ are annihilation operators of the spin and mechanical modes, respectively.

We perform spectroscopy of the coupled system using independent drive and detection channels for spin and membrane. The membrane vibrations are recorded by balanced homodyne detection using an auxiliary laser beam coupled to the cavity in orthogonal polarization. To drive the membrane, this beam is amplitude modulated. The spin precession is detected by splitting off a small portion of the coupling light on the path from spin to membrane. A radio-frequency (RF) magnetic coil drives the spin. We measure the amplitude and phase response of either system using a lock-in amplifier that demodulates the detector signal at the drive frequency (*32*). After spin-state initialization we simultaneously switch on coupling and drive and start recording. The drive frequency is kept fixed during each experimental run and stepped between consecutive runs.

Figure 2, A and B, shows the membrane's response in amplitude and phase, respectively. With the coupling beam off, it exhibits a Lorentzian resonance of linewidth $\gamma_m = 2\pi \times 0.3$ kHz, broader than the intrinsic linewidth due to optomechanical damping by the red-detuned cavity field (*36*). For the uncoupled spin oscillator (Fig. 2, C and D) with cavity off-resonant, we also measure a Lorentzian response of linewidth $\gamma_s = 2\pi \times 4$ kHz, broadened by the coupling light. When we turn on the coupling to the spin, the membrane resonance splits into two hybrid spin-mechanical normal modes. This signals strong coupling (*37*, *38*), where light-mediated coupling dominates over local damping. Fitting the well-resolved splitting yields $2g = 2\pi \times 6.1$ kHz, which exceeds the average linewidth $(\gamma_s + \gamma_m)/2 = 2\pi \times 2$ kHz and agrees with the expectation based on an independent calibration of the systems (*32*). A characteristic feature of the long-distance coupling is a finite delay $\tau$ between the systems. It causes a linewidth asymmetry of the two normal modes when $\Omega_s = \Omega_m$, which we observe in Fig. 2. The fits yield a value of $\tau = 15$ ns, consistent with the propagation delay of the light between the systems and the cavity response time.

We also observe normal-mode splitting in measurements of the spin (Fig. 2, C and D). Here, the combination of the broader spin linewidth with the much narrower membrane resonance results in a larger dip between the two normal modes and a larger phase shift, in analogy to optomechanically-induced transparency (*36*).

### *Energy exchange oscillations*

Having observed the spectroscopic signature of strong coupling, we now use it for swapping spin and mechanical excitations in a pulsed experiment. We start by coherently exciting the membrane to $\approx 2 \times 10^6$ phonons, a factor of 100 above its mean equilibrium energy, by applying an amplitude modulation pulse to the auxiliary cavity beam (Fig. 3A). At the same time, the spin is prepared in its ground state with $\Omega_s = \Omega_m$. The coupling beam is switched on at time $t$ = 0 μs and the displacements $X_s(t)$ and $X_m(t)$ of spin and membrane are continuously monitored via the independent detection. From the measured mean square displacements we determine the excitation number of each system (*32*). Figure 3C shows the excitation numbers as a function of the interaction time. The data show coherent and reversible energy exchange oscillations from the membrane to the spin and back with an oscillation period of $T \approx 150$ μs, in accordance with the value $\pi/g$ extracted from the observed normal-mode splitting. Damping limits the maximum energy transfer efficiency at time $T/2$ to about 40%.

The same experiment is repeated but with the initial drive pulse applied to the spin (Fig. 3, B and D). Here, we observe another set of exchange oscillations with the same periodicity, swapping an initial spin excitation of $n_s \approx 3 \times 10^5$ to the membrane and back. After the coherent dynamics have decayed, the systems equilibrate in a thermal state of $\approx 3 \times 10^3$ phonons, lower than the effective optomechanical bath of $1.5 \times 10^4$ phonons, demonstrating sympathetic cooling (*27*) of the membrane by the spin. The observed sympathetic cooling strength agrees with simulations using the experimentally determined parameters.

### *Parametric-gain dynamics*

So far we have explored Hamiltonian coupling of the membrane to a spin oscillator with positive effective mass, where the resonant interaction is of the beam-splitter type. If instead we reverse the magnetic field to $B_0 = -2.81$ G but keep the spin pumping direction the same, the collective spin is prepared in its highest energy state with $\bar{F}_x = +Nf$. In this case any excitation reduces the energy such that the spin oscillator has a negative effective mass (*17*) and $\Omega_s = -\Omega_m$ (Fig. 1B). The resonant term of $H_{\mathrm{eff}}$ is now the parametric-gain interaction (*36*) $H_{\mathrm{PG}} = \hbar g\left(b_s b_m + b_s^\dagger b_m^\dagger\right)$, which generates correlations between the two systems.

We investigate the dynamics generated by $H_{\mathrm{PG}}$ with the membrane driven by thermal noise. In order to quantify the development of spin-mechanical correlations, we determine slowly varying quadratures $\tilde{X}'_{s,m}$ and $\tilde{P}'_{s,m}$ of both systems as the cosine and sine components of the demodulated detector signals, respectively (*32*). Adjusting the demodulator phase allows us to find the basis with strongest correlations. Figure 4A shows histograms of the measured spin-mechanical correlations after an interaction time of $t$ = 100 μs. In each subplot, the dashed ellipse corresponds to the Gaussian 1-sigma contour of the measured histogram at $t$ = 0 μs while the solid line is the contour at $t$ = 100 μs. Compared to the uncorrelated initial state, the histograms show strong amplification along the axes $\tilde{X}_+ = \left(\tilde{X}'_s + \tilde{X}'_m\right)/\sqrt{2}$ and $\tilde{P}_- = \left(\tilde{P}'_s - \tilde{P}'_m\right)/\sqrt{2}$, and a small amount of thermal noise squeezing along $\tilde{X}_- = \left(\tilde{X}'_s - \tilde{X}'_m\right)/\sqrt{2}$ and $\tilde{P}_+ = \left(\tilde{P}'_s + \tilde{P}'_m\right)/\sqrt{2}$. The quadrature pairs $\tilde{X}'_s, \tilde{P}'_m$ and $\tilde{P}'_s, \tilde{X}'_m$ remain uncorrelated.

In the time evolution of the combined variances $\tilde{X}_\pm$ and $\tilde{P}_\pm$ (Fig. 4B), at $t$ = 0 all variances start from the same value indicating an uncorrelated state. As time evolves, the variances of $\tilde{X}_+$ and $\tilde{P}_-$ grow exponentially, demonstrating the dynamical instability in this configuration, while $\tilde{X}_-$ and $\tilde{P}_+$ are squeezed and reach a minimum at $t$ = 80 μs before they grow again. The exponential growth rate of $2\pi \times 4.5$ kHz is consistent with the value of $2g - (\gamma_m + \gamma_s)/2$ extracted from the normal-mode splitting. For comparison, we also show simulated variances for the experimental parameters which are given by the lines in Fig. 4B (*32*). Good agreement between data and simulation is found when accounting for a spin detector noise floor of $6 \times 10^3$ (solid lines). The dashed lines correspond to perfect detection and show thermal noise squeezing by 5.5 dB. Realizing the parametric-gain interaction by light-mediated coupling represents an important step toward generation of spin-mechanical entanglement by two-mode squeezing across macroscopic distances. Such entanglement is useful for metrology beyond the standard quantum limit (*1*).

### *Control of the loop phase*

Equipped with control over both the loop phase and the effective mass of the spin oscillator, we can access four different regimes of the spin-membrane coupling: two Hamiltonian configurations with $\phi = \pi$ and $\Omega_s = \pm\Omega_m$, and the two corresponding dissipative configurations where we set $\phi = 0$ by omitting the half-wave plate in the optical path from membrane to atoms (*32*). While the dynamics in these configurations are fundamentally different and have different quantum noise properties, we obtain simple equations of motion for the expectation values,

$$\ddot{X}_m + \gamma_m \dot{X}_m + \Omega_m^2 X_m = -g\Omega_m X_s\left(t-\tau\right) \tag{2}$$

$$\ddot{X}_s + \gamma_s \dot{X}_s + \Omega_s^2 X_s = -g\Omega_s \cos\left(\phi\right) X_m\left(t-\tau\right) \tag{3}$$

with the damped harmonic oscillations on the left and the delayed coupling terms on the right. These are derived from Heisenberg-Langevin equations of the full system (*32*) and reproduce the dynamics of the master equation in the limit $\tau \to 0$. Two distinct regimes can be identified. If $\Omega_s \cos\phi < 0$ we expect stable dynamics equivalent to a beam-splitter interaction. In the opposite case where $\Omega_s \cos\phi > 0$, the dynamics are equivalent to a parametric-gain interaction and unstable. A simultaneous sign reversal of $\Omega_s$ and a $\pi$-shift of $\phi$ should leave the dynamics invariant.

To probe the dynamics in these configurations, we record thermal noise spectra of the membrane while the spin Larmor frequency is tuned across the mechanical resonance $\Omega_m = 2\pi \times 1.957$ MHz. The Hamiltonian configuration with positive-mass spin oscillator is depicted in Fig. 5A, showing an avoided crossing at $\Omega_s = \Omega_m$ with frequency splitting $2g = 2\pi \times 5.9$ kHz, as in Fig. 2 above. The dashed lines are the calculated normal mode frequencies (*32*). The enhancement of the mechanical noise power for $\Omega_s < \Omega_m$ as compared to increased damping for $\Omega_s > \Omega_m$ is again a consequence of the finite optical propagation delay $\tau$ modifying the damping (*32*).

Switching to the dissipative regime with $\phi = 0$ renders the system unstable due to positive feedback of the coupled oscillations (Fig. 5B). Instead of an avoided crossing, the normal modes are now attracted and cross near $\Omega_s = 2\pi \times 1.953$ MHz, forming one strongly amplified and one strongly damped mode. The former leads to exponential growth of correlated spin-mechanical motion, finally resulting in limit-cycle oscillations which dominate the power spectrum. This ensues a breakdown of the coupled oscillator model, such that the observed spectral peak shifts toward the unperturbed mechanical resonance. Still, the data are in good agreement with the theoretical model.

In Fig. 5, C and D, we repeat the experiments of Fig. 5, A and B with negative-mass spin oscillator. The data show that Hamiltonian coupling with negative-mass spin oscillator produces similar spectra as dissipative coupling with positive-mass spin oscillator. In these configurations, the coupled system features an exceptional point (*39*) where the normal modes become degenerate (*40*) and define the squeezed and anti-squeezed quadratures. Conversely, dissipative coupling together with an inverted spin (D) shows an avoided crossing with similar parameters as in the Hamiltonian case (A). This equivalence at the level of the expectation values is expected to break down once quantum noise of the light becomes relevant. Due to interference in the loop, quantum back-action on the spin is suppressed in the Hamiltonian coupling configuration, but enhanced in the dissipative configuration.

A necessary condition for quantum back-action cancellation is destructive interference of the spin signal in the output field (*32*). Figure 5, E and F, shows homodyne measurements of coherent spin precession on the coupling beam output quadrature $X_L^{(\mathrm{out})}$ in time and frequency-domain, respectively. Toggling the loop phase between $\phi = 0$ and $\phi = \pi$, we observe a large interference contrast > 10 in the root-mean-squared (RMS) spin signal, showing that a spin measurement made by light in the first pass can be erased in the second pass. Optical loss of $1 - \eta^4 \approx 0.35$ inside the loop allows some information to leak out to the environment and brings in uncorrelated noise, limiting the achievable back-action suppression. Full interference in the output is still observed because the carrier and signal fields are subject to the same losses. Since this principle of quantum back-action interference is fully general, it could be harnessed as well for other optical or microwave photonic networks (*4*, *25*).

## Conclusion

The observed normal-mode splitting and coherent energy exchange oscillations establish strong spin-membrane coupling, where the coupling strength $g$ exceeds the damping rates of both systems (*37*). In order to achieve quantum-coherent coupling (*38*), $g$ must also exceed all thermal and quantum back-action decoherence rates. This will make it possible to swap non-classical states between the systems or to generate remote entanglement by two-mode squeezing. Thermal noise on the mechanical oscillator is the major source of decoherence in our room-temperature setup. We expect that modest cryogenic cooling of the optomechanical system to 4 K together with an improved mechanical quality factor of $>10^7$ (*41*) will enable quantum-limited operation (*32*). The built-in suppression of quantum back-action in the Hamiltonian configuration is a crucial feature of our coupling scheme. Interference of the two spin-light interactions reduces the spin's quantum back-action rate to $\gamma_{s,\mathrm{ba}} = (1 - \eta^4)\Gamma_s$ while it is $\gamma_{m,\mathrm{ba}} = \eta^2\Gamma_m$ for the membrane. Assuming thermal noise is negligible, the quantum cooperativity $C = 2g/(\gamma_{s,\mathrm{ba}} + \gamma_{m,\mathrm{ba}})$ can be optimized for a given one-way transmission $\eta^2$. We find an upper bound $C \le \eta\left(1+\eta^2\right)\big/\sqrt{1-\eta^4}$, reaching 2.7 for our current setup. The bound is achieved for an optimal choice of measurement rates $\Gamma_s/\Gamma_m = \eta^2/(1 -$

$\eta^4$), balancing the back-action on both systems. Further improvement is possible with a double-loop coupling scheme that also suppresses quantum back-action on the membrane (*26*). In this case, $C = \eta/(1 - \eta^2)$ at $\Gamma_s = \eta^2\Gamma_m$ is inversely proportional to optical loss, scaling more favorably at high transmission so that $C \approx 10$ can be reached for $\eta^2 = 0.9$.

Our results demonstrate a comprehensive and versatile toolbox for generating coherent long-distance interactions with light and open up a range of exciting opportunities for quantum information processing, simulation and metrology. The coupling scheme constitutes a coherent feedback network (*31*) that allows quantum systems to directly exchange, process and feed back information without the use of classical channels. The ability to create coherent Hamiltonian links between separate and physically distinct systems in a reconfigurable way significantly extends the available toolbox, not only for hybrid spin-mechanical interfaces (*9*, *29*) but quantum networks (*4*) in general. It facilitates the faithful processing of quantum information and the generation of entanglement between spatially separated quantum processors across a room temperature environment.

## REFERENCES AND NOTES


1. L. Pezzè, A. Smerzi, M. K. Oberthaler, R. Schmied, P. Treutlein, Quantum metrology with nonclassical states of atomic ensembles. *Rev. Mod. Phys.* **90**, 035005 (2018). doi:10.1103/RevModPhys.90.035005
2. C. Gross, I. Bloch, Quantum simulations with ultracold atoms in optical lattices. *Science* **357**, 995–1001 (2017). doi:10.1126/science.aal3837 Medline
3. T. D. Ladd, F. Jelezko, R. Laflamme, Y. Nakamura, C. Monroe, J. L. O'Brien, Quantum computers. *Nature* **464**, 45–53 (2010). doi:10.1038/nature08812 Medline
4. H. J. Kimble, The quantum internet. *Nature* **453**, 1023–1030 (2008). doi:10.1038/nature07127 Medline
5. R. Blatt, D. Wineland, Entangled states of trapped atomic ions. *Nature* **453**, 1008–1015 (2008). doi:10.1038/nature07125 Medline
6. R. Hanson, D. D. Awschalom, Coherent manipulation of single spins in semiconductors. *Nature* **453**, 1043–1049 (2008). doi:10.1038/nature07129 Medline
7. L. F. Buchmann, D. M. Stamper-Kurn, The quantum/classical transition in mediated interactions. *Ann. Phys.* **527**, 156–161 (2015). doi:10.1002/andp.201400150
8. P. Treutlein, C. Genes, K. Hammerer, M. Poggio, P. Rabl, in *Cavity Optomechanics: Nano- and Micromechanical Resonators Interacting with Light*, M. Aspelmeyer, T. J. Kippenberg, F. Marquardt, Eds. (Springer, 2014), pp. 327–351.
9. G. Kurizki, P. Bertet, Y. Kubo, K. Mølmer, D. Petrosyan, P. Rabl, J. Schmiedmayer, Quantum technologies with hybrid systems. *Proc. Natl. Acad. Sci. U.S.A.* **112**, 3866–3873 (2015). doi:10.1073/pnas.1419326112 Medline
10. C. Gardiner, P. Zoller, *Quantum Noise: A Handbook of Markovian and Non-Markovian Quantum Stochastic Methods with Applications to Quantum Optics* (Springer, 2004).
11. P. Lodahl, S. Mahmoodian, S. Stobbe, A. Rauschenbeutel, P. Schneeweiss, J. Volz, H. Pichler, P. Zoller, Chiral quantum optics. *Nature* **541**, 473–480 (2017). doi:10.1038/nature21037 Medline
12. D. E. Chang, J. S. Douglas, A. González-Tudela, C.-L. Hung, H. J. Kimble, *Colloquium* : Quantum matter built from nanoscopic lattices of atoms and photons. *Rev. Mod. Phys.* **90**, 031002 (2018). doi:10.1103/RevModPhys.90.031002
13. K. Lalumière, B. C. Sanders, A. F. van Loo, A. Fedorov, A. Wallraff, A. Blais, Input-output theory for waveguide QED with an ensemble of inhomogeneous atoms. *Phys. Rev. A* **88**, 043806 (2013). doi:10.1103/PhysRevA.88.043806
14. S. Ritter, C. Nölleke, C. Hahn, A. Reiserer, A. Neuzner, M. Uphoff, M. Mücke, E. Figueroa, J. Bochmann, G. Rempe, An elementary quantum network of single atoms in optical cavities. *Nature* **484**, 195–200 (2012). doi:10.1038/nature11023 Medline
15. P. Campagne-Ibarcq, E. Zalys-Geller, A. Narla, S. Shankar, P. Reinhold, L. Burkhart, C. Axline, W. Pfaff, L. Frunzio, R. J. Schoelkopf, M. H. Devoret, Deterministic Remote Entanglement of Superconducting Circuits through Microwave Two-Photon Transitions. *Phys. Rev. Lett.* **120**, 200501 (2018). doi:10.1103/PhysRevLett.120.200501 Medline
16. P. Kurpiers, P. Magnard, T. Walter, B. Royer, M. Pechal, J. Heinsoo, Y. Salathé, A. Akin, S. Storz, J.-C. Besse, S. Gasparinetti, A. Blais, A. Wallraff, Deterministic quantum state transfer and remote entanglement using microwave photons. *Nature* **558**, 264–267 (2018). doi:10.1038/s41586-018-0195-y Medline
17. B. Julsgaard, A. Kozhekin, E. S. Polzik, Experimental long-lived entanglement of two macroscopic objects. *Nature* **413**, 400–403 (2001). doi:10.1038/35096524 Medline
18. J. Hofmann, M. Krug, N. Ortegel, L. Gérard, M. Weber, W. Rosenfeld, H. Weinfurter, Heralded entanglement between widely separated atoms. *Science* **337**, 72–75 (2012). doi:10.1126/science.1221856 Medline
19. R. Riedinger, A. Wallucks, I. Marinković, C. Löschnauer, M. Aspelmeyer, S. Hong, S. Gröblacher, Remote quantum entanglement between two micromechanical oscillators. *Nature* **556**, 473–477 (2018). doi:10.1038/s41586-018-0036-z Medline
20. H. Krauter, C. A. Muschik, K. Jensen, W. Wasilewski, J. M. Petersen, J. I. Cirac, E. S. Polzik, Entanglement generated by dissipation and steady state entanglement of two macroscopic objects. *Phys. Rev. Lett.* **107**, 080503 (2011). doi:10.1103/PhysRevLett.107.080503 Medline
21. J. Majer, J. M. Chow, J. M. Gambetta, J. Koch, B. R. Johnson, J. A. Schreier, L. Frunzio, D. I. Schuster, A. A. Houck, A. Wallraff, A. Blais, M. H. Devoret, S. M. Girvin, R. J. Schoelkopf, Coupling superconducting qubits via a cavity bus. *Nature* **449**, 443–447 (2007). doi:10.1038/nature06184 Medline
22. M. Mirhosseini, E. Kim, X. Zhang, A. Sipahigil, P. B. Dieterle, A. J. Keller, A. Asenjo-Garcia, D. E. Chang, O. Painter, Cavity quantum electrodynamics with atom-like mirrors. *Nature* **569**, 692–697 (2019). doi:10.1038/s41586-019-1196-1 Medline
23. K. Baumann, C. Guerlin, F. Brennecke, T. Esslinger, Dicke quantum phase transition with a superfluid gas in an optical cavity. *Nature* **464**, 1301–1306 (2010). doi:10.1038/nature09009 Medline
24. N. Spethmann, J. Kohler, S. Schreppler, L. Buchmann, D. M. Stamper-Kurn, Cavity-mediated coupling of mechanical oscillators limited by quantum back-action. *Nat. Phys.* **12**, 27–31 (2015). doi:10.1038/nphys3515
25. A. F. Kockum, G. Johansson, F. Nori, Decoherence-Free Interaction between Giant Atoms in Waveguide Quantum Electrodynamics. *Phys. Rev. Lett.* **120**, 140404 (2018). doi:10.1103/PhysRevLett.120.140404 Medline
26. T. M. Karg, B. Gouraud, P. Treutlein, K. Hammerer, Remote Hamiltonian interactions mediated by light. *Phys. Rev. A* **99**, 063829 (2019). doi:10.1103/PhysRevA.99.063829
27. A. Jöckel, A. Faber, T. Kampschulte, M. Korppi, M. T. Rakher, P. Treutlein, Sympathetic cooling of a membrane oscillator in a hybrid mechanical-atomic system. *Nat. Nanotechnol.* **10**, 55–59 (2015). doi:10.1038/nnano.2014.278 Medline
28. P. Christoph, T. Wagner, H. Zhong, R. Wiesendanger, K. Sengstock, A. Schwarz, C. Becker, Combined feedback and sympathetic cooling of a mechanical oscillator coupled to ultracold atoms. *New J. Phys.* **20**, 093020 (2018). doi:10.1088/1367-2630/aadf20
29. C. B. Møller, R. A. Thomas, G. Vasilakis, E. Zeuthen, Y. Tsaturyan, M. Balabas, K.

Jensen, A. Schliesser, K. Hammerer, E. S. Polzik, Quantum back-action-evading measurement of motion in a negative mass reference frame. *Nature* **547**, 191–195 (2017). doi:10.1038/nature22980 Medline

30. R. A. Thomas *et al*., Entanglement between Distant Macroscopic Mechanical and Spin Systems. arXiv 2003.11310 [quant-ph] (25 March 2020).
31. J. Zhang, Y. Liu, R.-B. Wu, K. Jacobs, F. Nori, Quantum feedback: Theory, experiments, and applications. *Phys. Rep.* **679**, 1–60 (2017). doi:10.1016/j.physrep.2017.02.003
32. See supplementary materials.
33. K. Hammerer, A. S. Sørensen, E. S. Polzik, Quantum interface between light and atomic ensembles. *Rev. Mod. Phys.* **82**, 1041–1093 (2010). doi:10.1103/RevModPhys.82.1041
34. E. S. Polzik, K. Hammerer, Trajectories without quantum uncertainties. *Ann. Phys.* **527**, A15–A20 (2015). doi:10.1002/andp.201400099
35. J. D. Thompson, B. M. Zwickl, A. M. Jayich, F. Marquardt, S. M. Girvin, J. G. E. Harris, Strong dispersive coupling of a high-finesse cavity to a micromechanical membrane. *Nature* **452**, 72–75 (2008). doi:10.1038/nature06715 Medline
36. M. Aspelmeyer, T. J. Kippenberg, F. Marquardt, Cavity optomechanics. *Rev. Mod. Phys.* **86**, 1391–1452 (2014). doi:10.1103/RevModPhys.86.1391
37. S. Gröblacher, K. Hammerer, M. R. Vanner, M. Aspelmeyer, Observation of strong coupling between a micromechanical resonator and an optical cavity field. *Nature* **460**, 724–727 (2009). doi:10.1038/nature08171 Medline
38. E. Verhagen, S. Deléglise, S. Weis, A. Schliesser, T. J. Kippenberg, Quantum-coherent coupling of a mechanical oscillator to an optical cavity mode. *Nature* **482**, 63–67 (2012). doi:10.1038/nature10787 Medline
39. H. Xu, D. Mason, L. Jiang, J. G. E. Harris, Topological energy transfer in an optomechanical system with exceptional points. *Nature* **537**, 80–83 (2016). doi:10.1038/nature18604 Medline
40. N. R. Bernier, L. D. Tóth, A. K. Feofanov, T. J. Kippenberg, Level attraction in a microwave optomechanical circuit. *Phys. Rev. A* **98**, 023841 (2018). doi:10.1103/PhysRevA.98.023841
41. Y. Tsaturyan, A. Barg, E. S. Polzik, A. Schliesser, Ultracoherent nanomechanical resonators via soft clamping and dissipation dilution. *Nat. Nanotechnol.* **12**, 776–783 (2017). doi:10.1038/nnano.2017.101 Medline
42. T. M. Karg *et al*., Zenodo doi:10.5281/zenodo.3779295 (2020).
43. R. Grimm, M. Weidemüller, Y. B. Ovchinnikov, Optical Dipole Traps for Neutral Atoms. *Adv. At. Mol. Opt. Phys.* **42**, 95–170 (2000). doi:10.1016/S1049-250X(08)60186-X
44. G. A. Smith, S. Chaudhury, A. Silberfarb, I. H. Deutsch, P. S. Jessen, Continuous weak measurement and nonlinear dynamics in a cold spin ensemble. *Phys. Rev. Lett.* **93**, 163602 (2004). doi:10.1103/PhysRevLett.93.163602 Medline
45. B. Q. Baragiola, L. M. Norris, E. Montaño, P. G. Mickelson, P. S. Jessen, I. H. Deutsch, Three-dimensional light-matter interface for collective spin squeezing in atomic ensembles. *Phys. Rev. A* **89**, 033850 (2014). doi:10.1103/PhysRevA.89.033850
46. B. Vogell, T. Kampschulte, M. T. Rakher, A. Faber, P. Treutlein, K. Hammerer, P. Zoller, Long distance coupling of a quantum mechanical oscillator to the internal states of an atomic ensemble. *New J. Phys.* **17**, 043044 (2015). doi:10.1088/1367-2630/17/4/043044
47. P.-L. Yu, K. Cicak, N. S. Kampel, Y. Tsaturyan, T. P. Purdy, R. W. Simmonds, C. A. Regal, A phononic bandgap shield for high-*Q* membrane microresonators. *Appl. Phys. Lett.* **104**, 023510 (2014). doi:10.1063/1.4862031
48. M. Takeuchi, S. Ichihara, T. Takano, M. Kumakura, T. Yabuzaki, Y. Takahashi, Spin squeezing via one-axis twisting with coherent light. *Phys. Rev. Lett.* **94**, 023003 (2005). doi:10.1103/PhysRevLett.94.023003 Medline
49. P. T. Starkey, C. J. Billington, S. P. Johnstone, M. Jasperse, K. Helmerson, L. D. Turner, R. P. Anderson, A scripted control system for autonomous hardware-timed experiments. *Rev. Sci. Instrum.* **84**, 085111 (2013). doi:10.1063/1.4817213 Medline
50. L. Neuhaus *et al*., High power CEP-stable 2 µm source based on fiber-laser seeded Innoslab with 100-kHz to 1-MHz repetition rate. In *2017 European Conference on Lasers and Electro-Optics and European Quantum Electronics Conference* (Optical Society of America, 2017), paper CF_P_26.
51. V. B. Braginsky, Y. I. Vorontsov, K. S. Thorne, Quantum nondemolition measurements. *Science* **209**, 547–557 (1980). doi:10.1126/science.209.4456.547 Medline
52. S. G. Hofer, K. Hammerer, Entanglement-enhanced time-continuous quantum control in optomechanics. *Phys. Rev. A* **91**, 033822 (2015). doi:10.1103/PhysRevA.91.033822
53. L.-M. Duan, G. Giedke, J. I. Cirac, P. Zoller, Inseparability criterion for continuous variable systems. *Phys. Rev. Lett.* **84**, 2722–2725 (2000). doi:10.1103/PhysRevLett.84.2722 Medline
54. R. Simon, Peres-Horodecki separability criterion for continuous variable systems. *Phys. Rev. Lett.* **84**, 2726–2729 (2000). doi:10.1103/PhysRevLett.84.2726 Medline

ACKNOWLEDGMENTS

We are grateful to Gianni Buser for setting up the dipole trap and acknowledge discussions with Maryse Ernzer. **Funding:** This work was supported by the project "Modular mechanical-atomic quantum systems" (MODULAR) of the European Research Council (ERC) and by the Swiss Nanoscience Institute (SNI). KH acknowledges support through the cluster of excellence "Quantum Frontiers" and from DFG through CRC 1227 DQ-mat, projects A06. **Author contributions:** TMK, BG, KH and PT conceived the experiment. TMK and BG developed the theory, with input from KH and PT. TMK, BG, CTN and GLS built the experimental setup, and TMK took and analyzed the data, discussing with PT. TMK, PT and KH wrote the manuscript with input from other authors. KH and PT supervised the project. **Competing interests:** The authors declare no competing interests. **Data and materials availability:** All data needed to evaluate the conclusions in the paper are present in the figures of the paper. The data can be accessed at (*42*).

## SUPPLEMENTARY MATERIALS

science.sciencemag.org/cgi/content/full/science.abb0328/DC1
Supplementary Text
Figs. S1 to S4
Table S1
References (*43*–*54*)

27 January 2020; accepted 28 April 2020
Published online 7 May 2020
10.1126/science.abb0328

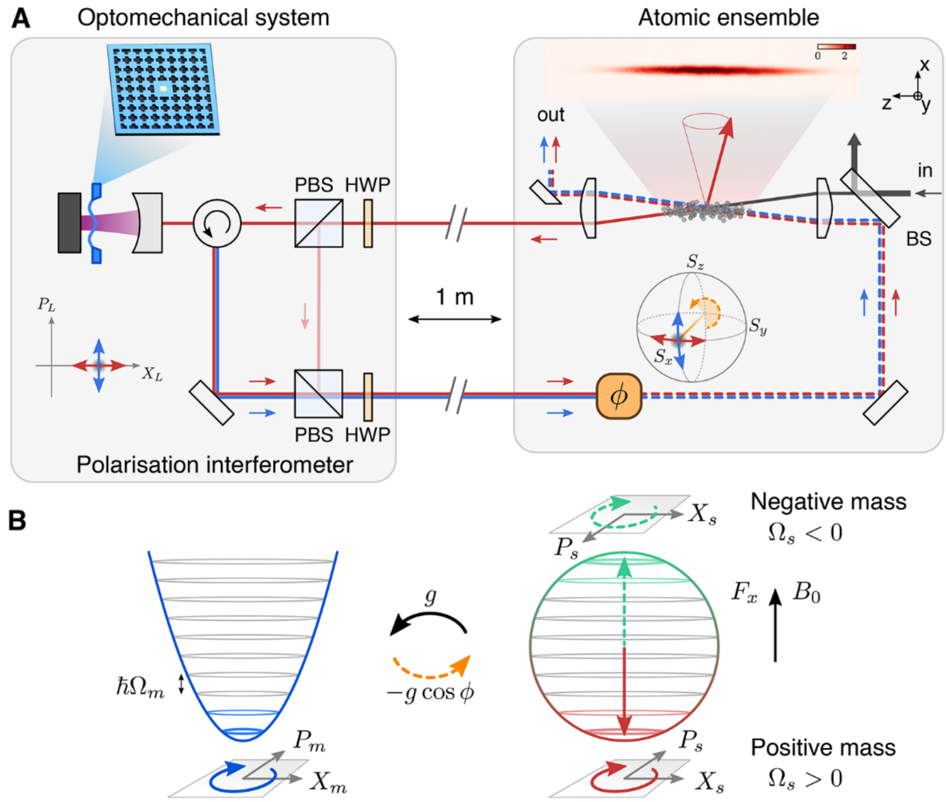


**Fig. 1. Schematic setup for long-distance Hamiltonian coupling.** (**A**) Cascaded coupling of an atomic spin ensemble (right) and a micromechanical membrane (left) by a free-space laser beam. The pictures show the silicon-nitride membrane embedded in a silicon chip with phononic crystal structure and a side-view absorption image of the atomic cloud (color bar: optical density). The laser beam first carries information from the atoms to the membrane and then loops back to the atoms such that it mediates a bidirectional interaction. A polarization interferometer (PBS: polarizing beam-splitter, HWP: half-wave plate) maps between the Stokes vector **S** defining the polarization state of light at the atoms and field quadratures $X_L$, $P_L$ relevant for the optomechanical interaction. The loop phase $\phi$ is controlled by a rotation of **S** by an angle $\phi$ in the optical path from the membrane to the atoms. (**B**) Effective interaction. The membrane vibration mode (harmonic oscillator) is coupled to the collective spin of the atoms (represented on a sphere). If the mean spin is oriented along an external magnetic field $B_0$ to either the south or north pole of the sphere, its small-amplitude dynamics can be mapped onto a harmonic oscillator with positive or negative mass, respectively. The relative phase of the spin-to-membrane coupling constant $g$ and the membrane-to-spin coupling constant $-g \cos \phi$ defines whether the effective dynamics are Hamiltonian ($\phi = \pi$) or dissipative ($\phi = 0$).

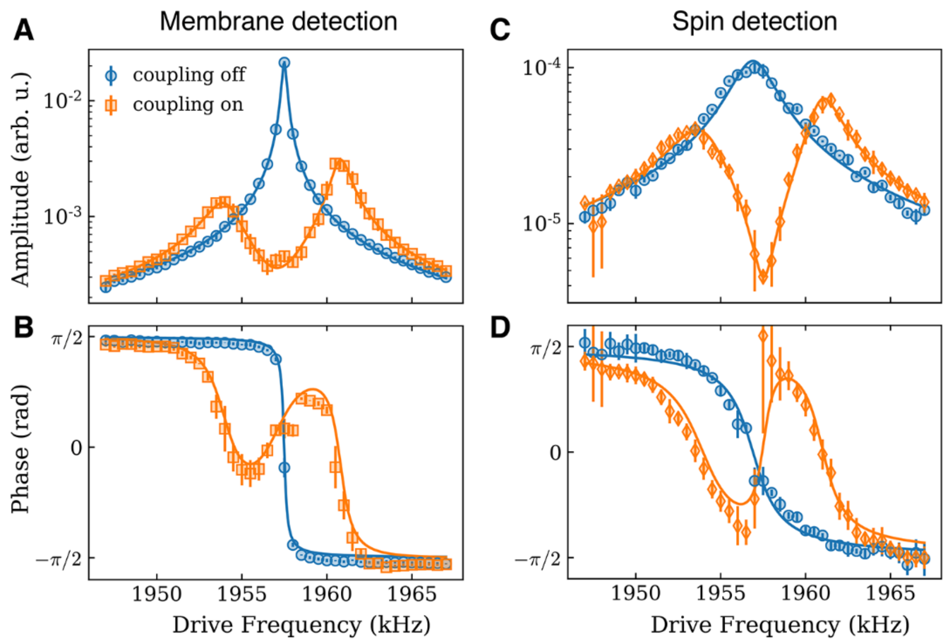


**Fig. 2. Observation of strong spin-membrane coupling.** Spectroscopy of the membrane (**A** and **B**) and the spin (**C** and **D**), both revealing a normal mode splitting if the coupling beam is on and the oscillators are resonant ($\Omega_s = \Omega_m$). For comparison we show the uncoupled responses of the membrane with coupling beam off [(A) and (B)] and of the spin with cavity off-resonant [(C) and (D)]. Lines are fits to the data with a coupled-mode model (*32*). Error bars are standard deviations of 3 independent measurements.

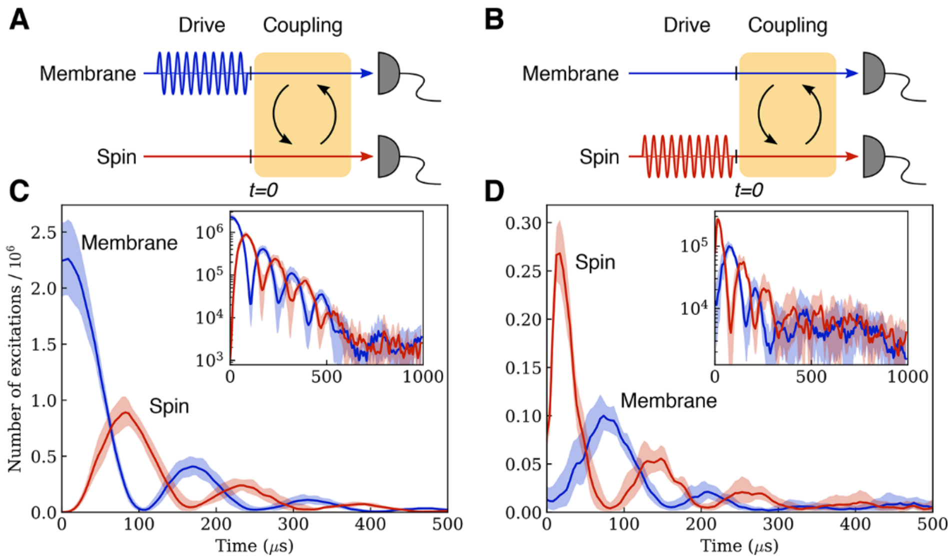


**Fig. 3. Time-domain exchange oscillations showing coherent energy transfer between spin and membrane.** (**A**) Pulse sequence for excitation of the membrane by radiation-pressure modulation via the auxiliary laser beam. (**B**) Pulse sequence for spin excitation with an external RF magnetic field. (**C**) Oscillations in the excitation numbers of membrane and spin as a function of the interaction time, measured using the pulse sequence in (A). (**D**) Data obtained with pulse sequence (B) and weaker drive strength than in (C). Here, the finite rise time of the spin signal at $t$ = 0 corresponds to the turn-on of the coupling beam, which is also used for spin detection. Insets in (C) and (D) show the same data on a log-scale. Lines and shaded areas represent the mean and one standard deviation of five measurements, respectively.

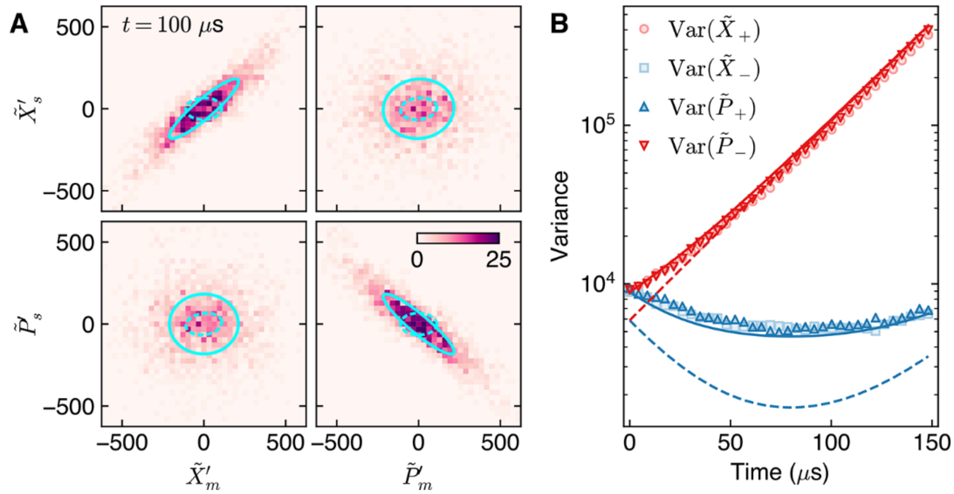


**Fig. 4. Dynamics of the parametric-gain interaction with thermal noise averaged over 2000 realizations.** (**A**) Phase space histograms showing correlations between the rotated spin and membrane quadratures after 100 μs of interaction time. The solid (dashed) ellipses enclose regions of one standard deviation at $t$ = 100 μs ($t$ = 0 μs). (**B**) Variances of the combined quadratures $\tilde{X}_\pm$ and $\tilde{P}_\pm$ as a function of interaction time. Exponential increase is observed for quadratures $\tilde{X}_+$ and $\tilde{P}_-$ while noise reduction is measured for $\tilde{X}_-$ and $\tilde{P}_+$. The solid lines are a simulation of the corresponding variances including a spin detector noise floor of $6 \times 10^3$, while the dashed lines assume noise-free detection.

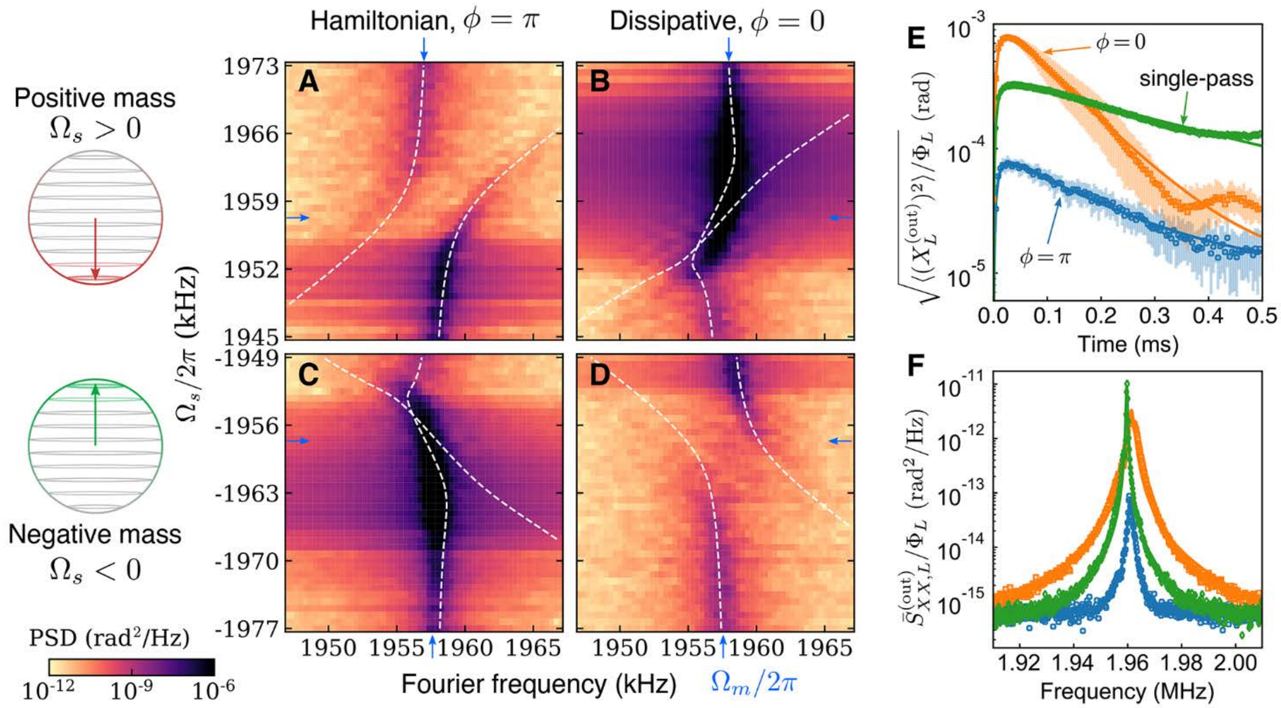


**Fig. 5. Control of the loop phase.** (**A** to **D**) Density plots of the membrane's thermal noise spectra in four different regimes, with membrane Fourier frequency on the horizontal axis ($\Omega_m$ indicated by blue arrows) and spin frequency $\Omega_s$ (controlled by magnetic field) on the vertical axis. Dashed white lines are the calculated normal mode frequencies. (A) Hamiltonian coupling with positive-mass spin oscillator (beam-splitter interaction): an avoided crossing is observed. (B) Dissipative coupling with positive-mass spin oscillator: level attraction and unstable dynamics at the exceptional point. (C) Hamiltonian coupling with negative-mass spin oscillator (parametric-gain interaction): unstable dynamics and an exceptional point. (D) Dissipative coupling with negative-mass spin oscillator: observation of an avoided crossing. (**E**) Atomic spin signal (RMS amplitude) on the output light after pulsed excitation: constructive (destructive) interference of the two atom-light interactions is observed for $\phi = 0$ ($\phi = \pi$) compared to a single-pass interaction. The membrane is decoupled by detuning the cavity. Error bars are standard deviations of 25 repetitions. (**F**) Frequency-domain power spectra correspond to the data of (E).

# Light-mediated strong coupling between a mechanical oscillator and atomic spins 1 meter apart

Thomas M. Karg, Baptiste Gouraud, Chun Tat Ngai, Gian-Luca Schmid, Klemens Hammerer and Philipp Treutlein

published online May 7, 2020



*Science* (print ISSN 0036-8075; online ISSN 1095-9203) is published by the American Association for the Advancement of Science, 1200 New York Avenue NW, Washington, DC 20005. The title *Science* is a registered trademark of AAAS.